Biomass burning related ammonia emissions promoted a self-amplifying loop in the urban environment in Kunming (SW China)

Yunhong Zhou [a,b], Nengjian Zheng [d], Li Luo [d], Jingjing Zhao [a,b], Linglu Qu [e], Hui Guan [a], Hongwei Xiao [d], Zhongyi Zhang [d], Jing Tian [a,b], Huayun Xiao [c,*]

[a] State Key Laboratory of Environmental Geochemistry, Institute of Geochemistry, Chinese Academy of Sciences, Guiyang, 550081, China
[b] University of Chinese Academy of Sciences, Beijing, 100049, China
[c] School of Environmental Science and Engineering, Shanghai Jiao Tong University, Shanghai, 200240, China
[d] Key Laboratory of the Causes and Control of Atmospheric Pollution, East China University of Technology, Nanchang, 330000, China
[e] State Key Laboratory of Environmental Criteria and Risk Assessment, Chinese Research Academy of Environmental Sciences, Beijing, 100012, China

HIGHLIGHTS

- A self-amplifying loop was proposed when the concentration of NH_4^+ in $PM_{2.5}$ elevated in late autumn in Kunming.
- Biomass burning related ammonia emissions significantly enhanced during slightly polluted days.
- Increased biomass burning emissions in Kunming were related to ammonia emissions from local area and regional transport.

GRAPHICAL ABSTRACT
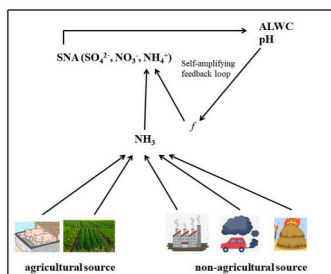
ARTICLE INFO

ABSTRACT

Particulate ammonium (NH_4^+) is one of the most important inorganic components in aerosol. The concentrations of NH_4^+ in $PM_{2.5}$ significantly increased when $PM_{2.5}$ levels elevated. Increased understanding of the atmospheric processes and sources of ambient ammonia is an effective way to control atmospheric ammonia and tackle air pollution problems. This study focused on the concentration and nitrogen stable isotopic composition of particulate NH_4^+ in $PM_{2.5}$ in a southwest typical plateau city, Kunming. The trend in NH_4^+ concentrations was parallel to the trend in $PM_{2.5}$ levels, with obviously increased concentrations observed in November. Aerosol pH and liquid water content (ALWC) were synchronously simulated by the ISORROPIA-II model. And the ammonia gas-particle conversion ratio (f) was calculated for each day. Then, we proposed that a self-amplifying feedback mechanism of NH_4^+ formation was associated with the variations of ALWC, pH, and the ammonia gas-particle conversion ratio. Based on the inverse analysis of the nitrogen isotopic composition of particulate NH_4^+, the corresponding $\delta^{15}N$ values of initial ambient NH_3 were estimated to be $-27.4‰–15.3‰$, with an average of $-8.1 \pm 8.3‰$. Results from Back trajectory analysis, PSCF analysis, and isotope-based source apportionment of NH_3 shed light on source compositions and potential source regions, indicating that, in the study area, ambient NH_3 during slightly polluted days were dominated by biomass burning emissions, which might have been originated from local emissions and regional transport process in late autumn.

1. Introduction

Ambient ammonia (NH_3) is a major nitrogen-containing species and an abundant alkaline gas in the atmosphere. It plays a vital role in local and regional scale tropospheric chemistry by acting as an important precursor to ammonium salts in $PM_{2.5}$ (Seinfeld et al., 2006). Fine particulate ammonium salts (including ammonium sulfate and ammonium nitrate) are the major components of inorganic aerosols and typically constitute 20–80% of atmospheric fine particulate matter (Huang et al., 2014). Ammonium nitrate has a lower deliquescence relative humidity (DRH = 61.8%) than ammonium sulfate (DRH = 79.9%) (Seinfeld et al., 2006). Ambient environmental factors significantly affect the formation of ammonium salt. Ambient NH_3 is crucial in controlling aerosol pH by suppressing the production of particle hydronium (Wang et al., 2016). NH_3 emission control has recently been proposed as a potential strategic option to mitigate severe haze pollution in China due to its role in facilitating secondary $PM_{2.5}$ formation (Liu et al., 2019). However, there are still substantial gaps in our knowledge on the sources and formation processes of volatile species NH_4^+ in $PM_{2.5}$.

Ambient NH_3 is composed of a mixture of agricultural sources (mainly from fertilizer application and livestock manure) and non-agricultural sources (emissions from combustion). Bottom-up ammonium emissions inventories indicate that livestock manure and fertilizer application were the top two major sources, contributing up to 80–90% of the total emissions in China (Huang et al., 2012; Kang et al., 2016). In Yunnan province of China, atmospheric ammonia emissions in 2006 were mainly composed of fertilizer (57 Gg) and livestock (228.1 Gg) emissions (Huang et al., 2012). However, the top-bottom isotopic source tracing methods have indicated that vehicle emissions play an important role in the megacity of Shanghai as a source of ambient ammonia (Chang et al., 2016b). Moreover, fossil fuel-related emissions were reported to dominate NH_3 pollution in severe haze episodes in 2013 in Beijing (Pan et al., 2016) and in urban cities of Northern China Plain in the autumn of 2017 (Zhang et al., 2020b).

Stable nitrogen isotope techniques can be used to identify the sources of atmospheric NH_3 by comparison with $\delta^{15}N$ of NH_3 in certain emission sources (Chang et al., 2016a, 2016b, 2019b; Pan et al., 2016, 2018b). The variation in the ranges of isotopic values of particulate NH_4^+ offers an effective approach for source apportionment of ambient NH_3 in an urban environment. In the process of gas-to-particle conversion of ambient ammonia, kinetic fractionation of nitrogen isotope initially occurs; a unidirectional neutralization reaction occurs with atmospheric $NH_3(g)$ and $H_2SO_4(g)$ during the particle nucleation process under non-equilibrium conditions. In this process, different isotope diffusion rates caused by mass differences between heavy and light atoms lead to the kinetic isotopic effect (KIE). The diffusion rate ratio between light and heavy isotopes of different ammonia isotopologues is $\sqrt{17/18} = 0.972$. In this situation, the isotopic composition of nitrogen in the initial converted particulate NH_4^+ would be approximately $-28‰$ lower than that in the ambient NH_3 (Pan et al., 2016). Heaton et al. (1997) conducted an experiment which showed that the $\delta^{15}N$ value of instantaneously formed NH_4^+ was approximately $-10‰$ lower than the initial NH_3 in the first few minutes. The negative $\delta^{15}N$ value of NH_4^+ verified the existence of the KIE at the initial stage of the reaction. With growth in particulate matter, the equilibrium condition between gas NH_3 and particle NH_4^+ can be rapidly reached, and the KIE can be masked. Heavier ammonia molecules prefer to be preserved in the stable particulate NH_4^+ phase, which causes isotopic fractionation of about $+33‰$ between ambient NH_3 and particle NH_4^+. Therefore, the $\delta^{15}N$ value of ambient NH_3 can be calculated using the $\delta^{15}N$ value of NH_4^+ in $PM_{2.5}$ based on the isotopic mass balance, when assuming a well-mixed system between gas NH_3 and particulate NH_4^+ and the influence of initial NH_4^+ is ignored.

$$\delta_{NH_3} = \delta_{NH_4^+} - \varepsilon_{NH_4^+ - NH_3} * (1 - f) \tag{1}$$

where $\varepsilon_{NH_4^+ - NH_3}$ is the enrichment factor when the equilibrium condition is reached. $\varepsilon(aerosol - gas) = 12.4678 * 1000/(T + 273.5) - 7.6694$, when $T = 295.15 K$, $\varepsilon_{NH_4^+ - NH_3} \approx 34‰$. This value is consistent with the equilibrium isotopic enrichment factors of $+33‰$ and $+34‰$ between ambient NH_3 and particle NH_4^+ at 25 °C in previous studies when the equilibrium condition was reached (Heaton et al., 1997; Kirshenbaum et al., 1947).

The parameter f is the key to determining $\delta^{15}N–NH_3$. If the concentrations of ambient NH_3 and particulate NH_4^+ are measured simultaneously, f can be directly obtained (Wu et al., 2019). However, if data on the ambient NH_3 mass concentration are missing, the atmospheric transport model (like WRF-Chem model and WRF-CMAQ model) can be run to simultaneously simulate NH_3 and NH_4^+ during the study period, and f can be calculated based on the analog value obtained (Pan et al., 2016, 2018a, 2018b). It has been reported that particle acidity or pH is a fundamental property which affects atmospheric particulate chemistry, such as the gas-particle partitioning of semi-volatile and volatile species (e.g., NH_3/NH_4^+, HCl/Cl^- and HNO_3/NO_3^-), the formation of secondary inorganic and organic aerosols, and the dissolution of metallic elements (Guo et al., 2016; Seinfeld et al., 2006). In other words, gas-to-particle partitioning of ammonia can be well constrained by aerosol pH. Direct measurement of aerosol pH is challenging due to the small size and nonideality of the chemical species in solvated aerosols. However, the ISORROPIA-II thermodynamic model, which is based on the measurement of gas and particulate phase species, has been widely applied to the estimation of aerosol pH, and can be used to understand its role in aerosol nitrate and ammonium partitioning and source (Guo et al., 2016, 2017a). Previous studies have reported that the air quality in Kunming was better than most other megacities in China (Yin et al., 2017). However, in recent years, haze pollution has been found to have an increasing tendency in Kunming city, so what caused such a phenomenon is expected to be further explored. Figuring out the atmospheric processes and sources of particulate NH_4^+ is the basis to provide insight into effective government policies and regulations to improve air quality. So far, it's the first study focused on the isotopic composition of ammonium in $PM_{2.5}$ for the southwest city in China. In this study, (1) the $\delta^{15}N–NH_4^+$ values and the concentrations of water soluble inorganic ions (WSIIs) in $PM_{2.5}$ in autumn were analyzed in Kunming; (2) the ISORROPIA II model was run to simulate pH and aerosol liquid water content (ALWC) in $PM_{2.5}$, and the relationships between different compositions were further studied; (3) the initial $\delta^{15}N–NH_3$ value was estimated based on stable nitrogen isotopic fractionation via ammonia gas-to-particle conversion. Then, the isotopic mixing model was applied to apportion the sources of NH_3 in the urban atmosphere; and (4) back trajectory model simulation was performed to investigate the possible gas pollutant transport process.

2. Methods

2.1. Sample collection and chemical analysis

Famous as "spring city", Kunming is located in southwest China in the central Yunnan-Guizhou plateau. It belongs to a mountain monsoon climate characteristic of the low latitude plateau in the north subtropical zone. It is surrounded by mountains on three sides and Dianchi Lake to the south. Due to its location in the low latitude plateau, Kunming has a "four seasons like spring" climate. Kunming covers an area of 21,400 km^2 and has a population of about 6.67 million. Affected by both the Indian monsoon and East Asia monsoon, the rainy season in Kunming occurs from May to October.

$PM_{2.5}$ samples were collected with a high flow rate (1.05 ± 0.03 m^3

min^{-1}) KC-1000 sampler (Laoshan Institute for Electronic Equipment, Qingdao, China), which was set up on the top of a teaching building at Kunming University of Science and Teaching (102.70°N, 25.06°E) (Zhou et al., 2020). Daily PM$_{2.5}$ samples were collected using quartz filters (8 × 10 inch, Tissuquartz™ Filters, 2500 QAT-UP, Pallflex, Washington, USA) and were immediately stored at the refrigerator at −20 °C until chemical analysis. Sampling started at 9:00 a.m. and lasted for 23.5 h. The study site is located in the center area of Kunming, surrounded by heavily trafficked roads and dense residential buildings; there are no industrial emission sources nearby.

The concentrations of WSIIs in PM$_{2.5}$ in autumn and the δ^{15}N–NH$_4^+$ values in late autumn (between September 1 and November 30) were analyzed in Kunming. And the analysis of WSIIs mass concentrations had been described in detail in previous study (Zhou et al., 2020). The isotopic compositions of NH$_4^+$ (δ^{15}N–NH$_4^+$) were determined based on a chemical method that involved analysis of the isotope of nitrous oxides (N$_2$O) after a series of chemical conversions of the specific compound (Zhang et al., 2007). In brief, dissolved NH$_4^+$ in aerosol samples was initially oxidized to NO$_2^-$ using the newly prepared alkaline hypobromite (BrO$^-$). Then sodium arsenite was added to consume excess BrO$^-$, and the yield was verified by colorimetric NO$_2^-$ determination. Next, NO$_2^-$ was further reduced to N$_2$O by 1:1 sodium azide (NaN$_3$) and acetic acid buffer solution. Then, the produced N$_2$O was analyzed using a purge and cryogenic trap system (Gilson GX-271, Isoprime Ltd., Cheadle Hulme, UK), coupled with an isotope ratio mass spectrometer (PT-IRMS) (Isoprime 100, Isoprime Ltd., Cheadle Hulme, UK). In order to correct for any machine drift and procedural blank contributions, international NH$_4^+$ standards (IAEA N1, IAEA N$_2$ and USGS 25 with δ^{15}N values of 0.4‰, 20.3‰, and −30.4‰, respectively) were inserted into sample test sequences. Replicate NH$_4^+$ standards (n = 5) varying in concentration had a standard deviation of 0.3‰. Standard regressions were performed based on the known isotopic values of international standards and the measured standard ^{15}N values. The coefficient of determination (R^2) of the regression line was 0.999.

Meteorological data (temperature and relative humidity) in the autumn of 2017 in Kunming were obtained from National Meteorological Information Center (http://data.cma.cn/data/).

2.2. Backward trajectory analysis

NOAA's TrajStat program (Almeida et al., 2015; Liu et al., 2016; Zhang et al., 2014) was used to compute 72-h air mass back trajectories for all sampling days (from September 1, 2017 to November 30, 2017). Meteorological NCEP GDAS (Global Data Assimilation System) data compiled for this study can be found at the National Oceanic and Atmospheric Administration Laboratory (NOAA ARL) on the website (ftp://arlftp.arlhq.noaa.gov/archives). The back trajectories started at 16:00 UTC (Beijing time is 00:00), the arrival level of the air masses was set at 1000 m above the study site. In this study, trajectories were classified optimally using the clustering method for different months. Three clustering trajectories were obtained for each month.

PSCF (potential source contribution function) analysis of ambient NH$_3$ was performed based on the set criterion values (the mean concentrations of NH$_4^+$ in PM$_{2.5}$) and daily backward trajectories. This method has been widely used in the estimation of potential source regions. All 24-h endpoints from the back trajectories were classified into 1°*1° latitude and longitude grid cells. The PSCF values for the grid cells were calculated by counting the trajectory segment endpoint that terminated within each grid cell. The PSCF value for the ijth cell was defined as:

$$PSCF_{ij} = m_{ij} / n_{ij}$$

where m$_{ij}$ is the number of endpoints for the same cell having arrival times at the sampling site corresponding to particle NH$_4^+$ concentrations higher than the set criterion values. n$_{ij}$ represents the total number of

endpoints in the grid cell. To reduce the effect of small values of n$_{ij}$, the PSCF values were multiplied by an arbitrary weight function W_{ij} to better reflect the uncertainty in the values of these cells (Polissar et al., 1999). The weighting function reduced the PSCF values when the total number of endpoints in a particular cell was less than about three times the average value of the end points per cell. In this case, W_{ij} was defined as:

$$W_{ij} = \begin{cases} 1.00; n_{ij} > 3n_{ave} \\ 0.70; 3n_{ave} > n_{ij} > 1.5n_{ave} \\ 0.40; 1.5n_{ave} > n_{ij} > n_{ave} \\ 0.20; n_{ave} > n_{ij} \end{cases} \tag{2}$$

2.3. Thermodynamic model

The ISORROPIA II model is a computationally efficient thermodynamic equilibrium model used to determine the composition and phase state for K$^+$-Ca^{2+}-Mg^{2+}-NH$_4^+$-Na$^+$-SO$_4^{2-}$-NO$_3^-$-Cl$^-$-H$_2$O aerosols when it assumes that thermodynamic equilibrium is achieved between fine particles and gases for four pairs of semivolatile inorganic species (NH$_3$/NH$_4^+$, HNO$_3$/NO$_3^-$, HCl/Cl$^-$ and water(g)/water (aq)) (Fountoukis and Nenes, 2007). The ISORROPIA II can calculate in forward mode in which T, RH and the concentration of gas + aerosols of each pair of semivolatile inorganic species are known, while in reverse mode only T, RH and concentrations of aerosols are known. In this study, the ISORROPIA II model was used iteratively until the output composition was similar to the analyzed values of fine particles; the details can be obtained elsewhere (Zhang et al., 2020b).

2.4. NH$_3$–NH$_4^+$ partitioning

Equilibrium process between NH$_3$ and NH$_4^+$ can be described as follows

$$NH_{3(g)} \leftrightarrow NH_3, K_1 \tag{3}$$

$$NH_3 + H^+ \leftrightarrow NH_4^+, K_2 \tag{4}$$

when the chemical reaction equilibriums were reached, the equilibrium constants are described as

$$K_1 = \gamma_{(NH_3)}[NH_3] / P_{NH_3} \tag{5}$$

$$K_2 = \frac{\gamma_{(NH_4^+)}[NH_4^+]}{\gamma_{(NH_3)}[NH_3]\gamma_{(H^+)}[H^+]} \tag{6}$$

where K_i is equilibrium constant of the ith chemical reaction, $1/K_i$ is NH$_3$ Henry's law constant, γ_i represents activity coefficient of the ith species , $P_{(NH_3)}$ is the partial pressure of NH$_3$ in the air, and $[X]$ represents concentrations of X species.

Total particle-phase ammonium $[T_{NH4}]$:

$$[T_{NH4}] = [NH_3] + [NH_4^+] \tag{7}$$

Under the ideal gas law

$$c(NH_3) = P_{(NH_3)} / RT \tag{8}$$

where $c(x)$ is concentration of x per volume of air. R = 8.314 J/mol*K. The gas-particle partition of ammonium can be described as:

$$f(T_{NH4}) = \frac{c(T_{NH4})}{c(T_{NH4}) + c(NH_3)} \tag{9}$$

Combined with Equations (1) and (2),$\varepsilon(T_{NH4})$ can be written as follows

$$f(T_{NH4}) = \frac{[NH_4^+]}{[NHx]} = \frac{[T_{NH4}]W_i}{[T_{NH4}]W_i + c(NH_3)}$$

$$= \frac{\left(\frac{\gamma_{(H^+)}[H^+]}{\gamma_{(NH_4^+)}} + \frac{1}{K_2\gamma_{(NH_3)}}\right)K_1 K_2 W_i RT}{1 + \left(\frac{\gamma_{(H^+)}[H^+]}{\gamma_{(NH_4^+)}} + \frac{1}{K_2\gamma_{(NH_3)}}\right)K_1 K_2 W_i RT} \quad (10)$$

$\frac{\gamma_{(H^+)}[H^+]}{\gamma_{(NH_4^+)}} \gg \frac{1}{K_2\gamma_{(NH_3)}}$, we neglect $\frac{1}{K_2\gamma_{(NH_3)}}$ part and set $K1*$ $K2$ as K, the equation above is transformed into:

$$f(T_{NH4}) = \frac{[T_{NH4}]W_i}{[T_{NH4}]W_i + c(NH_3)} \cong \frac{\frac{\gamma_{(H^+)}[H^+]}{\gamma_{(NH_4^+)}}KW_iRT}{1 + \frac{\gamma_{(H^+)}[H^+]}{\gamma_{(NH_4^+)}}KW_iRT}$$

$$\cong \frac{\frac{\gamma_{(H^+)}[H^+]}{\gamma_{(NH_4^+)}}KW_iRT \times 0.987 \times 10^{-14}}{1 + \frac{\gamma_{(H^+)}[H^+]}{\gamma_{(NH_4^+)}}KW_iRT \times 0.987 \times 10^{-14}} \quad (11)$$

$$\cong \frac{\frac{\gamma_{(H^+)} \times 10^{-pH}}{\gamma_{(NH_4^+)}}KW_iRT \times 0.987 \times 10^{-14}}{1 + \frac{\gamma_{(H^+)} \times 10^{-pH}}{\gamma_{(NH_4^+)}}KW_iRT \times 0.987 \times 10^{-14}}$$

where 0.987 is the correction value from the conversion from 1 atm to 1 bar and W_i unit is μg m^{-3}. K can be calculated according to

$$\ln(K) = 25.393 - 10373.6(1/T_r - 1/T) + 4.131(T_r/T - (1 + \ln(T_r/T))) \quad (12)$$

where T_r is the reference temperature of 298.15 K. $\gamma_{(H^+)}/\gamma_{(NH_4^+)} = 1.9$ (Guo et al., 2017a).

2.5. Stable isotopic mixing model

A Bayesian stable isotopic mixing model was utilized to calculate the relative fractions of different atmospheric NH_3 sources to the total NH_3 content. This model can effectively solve the uncertainties associated with multiple sources, fractionations, and measured isotope signatures (Davis et al., 2015). This method has been widely used in atmospheric source apportionment. It iteratively computes using feasible isotopic signatures of different endmembers with fractions sum to 100%. The Bayesian model is more likely to give accurate prediction results than the linear mixing model due to the uncertainty between the N isotopic signatures of multiple sources (Chang et al., 2016a). In this study, an updated software package, SIMMR, for stable isotopic mixing models based on Bayesian methodology, was installed in R and was used to generate probability estimates of source proportions. The output data exported from the mixing model for each analysis were used to calculate mean ± SD values. In this study, ambient NH_3 was primarily assumed to be derived from four different sources. Emissions from livestock and fertilizers were classified as agricultural sources with mean $\delta^{15}N$ values of $-29.1 \pm 1.7‰$ ($-31.7‰$ to $-27.1‰$) and $-50 \pm 1.8‰$ ($-52.0‰$ to $-47.6‰$), respectively (Chang et al., 2016a). And emissions from vehicle exhaust and coal combustion were combined as fossil fuel sources attributed to the variation in the ranges of $\delta^{15}N$ values of these two sources lie in a similar region compared to other sources (coal combustion: 7 to 2‰, Freyer (1978) and vehicle exhaust: 4.6 to $-2.2‰$ Felix et al. (2013)). In addition, Kawashima and Kurahashi (2011) suggested that the $\delta^{15}N–NH_3$ value of biomass burning was 12‰. While ambient NH_3 can also originated from other sources (such as from volcanoes, plants, and the marine environment), these sources were ignored due to the focus on the urbanized, inland region of Kunming.

3. Results and discussion

3.1. Basic characteristics in $PM_{2.5}$

3.1.1. $PM_{2.5}$ levels and concentrations of WSIIs in $PM_{2.5}$

As shown in Fig. 1 and Fig. 2, the mass concentrations of $PM_{2.5}$ in Kunming fluctuated between 10.0 and 74.0 μg/m^3 (arithmetic mean value: 26.9 ± 14.1 μg/m^3) during the autumn of 2017; this fluctuation strongly correlated with meteorological factors. It's found in previous studies that the heavy aerosol pollution in most regions of China was associated with stagnant air conditions, which were characterized with lower temperature, weak wind and higher relative humidity (Pan et al., 2016; Wang et al., 2016). In this study, $PM_{2.5}$ levels showed significant negative correlation with daily temperature (R = -0.51, p < 0.01) and wind speed (R = -0.23, p < 0.05), but they were poorly correlated with wind speed RH. Rainfall evets, frequent occurred in September and October, were one of the most effective ways to scavenge particulate matter from the atmosphere. In addition, the boundary layer height and wind shear were also reported to be associated with the dispersion of ground-level aerosol, thereby altering the concentration of $PM_{2.5}$ (Liu et al., 2018; Lou et al., 2019; Su et al., 2020; Zhang et al., 2020a). The average concentration of total WSIIs was 13.4 ± 7.0 μg/m^3 (varied from 3.4 to 35.9 μg/m^3), accounting for 49.7% of the total $PM_{2.5}$ mass. During the study period, the concentrations of $PM_{2.5}$ and water soluble inorganic ions (WSIIs) increased significantly in November, when there were several slightly polluted haze events occurred. The mass concentrations of NH_4^+ in $PM_{2.5}$ over the whole study period varied from 0.05 to 6.2 μg/m^3, with an average of 2.1 ± 1.2 μg/m^3. Particulate NH_4^+ is one of the most abundant inorganic species in aerosols, accounting for 8.2% of the total $PM_{2.5}$ mass. The monthly average concentrations of NH_4^+ were 1.7 ± 0.6 μg/m^3, 1.9 ± 0.9 μg/m^3, and 2.8 ± 1.5 μg/m^3 in September, October, and November, respectively. The trend in NH_4^+ concentrations was parallel to the trend in $PM_{2.5}$ levels, with obviously increased concentrations observed in November. The mean mole ratio of $NH_4^+/(NO_3^- + 2*SO_4^{2-})$ were 0.72 ± 0.09, $0\ 0.75 \pm 0.18$ and 0.76 ± 0.13, respectively, suggesting that the acidic species (H_2SO_4 and HNO_3) were not fully neutralized by gas NH_3. In this study, the clean and slightly polluted periods were divided based on the concentrations of $PM_{2.5}$ (45 μg/m^3).

Back-trajectory clustering results of air masses in Kunming were calculated for each month in autumn (Fig. 3). In November, trajectories derived from southwest and south Kunming accounted for 70% and 30% of the total trajectories, respectively. Back trajectory analysis indicated that source regions in November were such different compared to September and October. Thus, long-distance transport might be one main reason underlying the gradual increase in particulate NH_4^+ concentrations in $PM_{2.5}$ in late autumn. In addition, fire spots distributed around southwest Kunming and southeast Asia were obviously concentrated in November, which indicated that long-distance air mass transport was likely brought air pollutants emitted from biomass burning to Kunming. Further, PSCF also identified "hot spots" in Burma, southwest Yunnan and local areas of Kunming in November, suggesting local emissions and regional transport both contributed to particulate ammonium in Kunming in November.

3.1.2. Aerosol pH

Daily aerosol pH values in Kunming during late autumn were calculated by the ISORROPIA-II model. The results indicated that the fine particles were moderately acidic in this southwest plateau city of China, with pH values ranging between 1.6–3.8, and with a mean pH of 2.9 ± 0.4. The correlated aerosol liquid water contents (ALWC) also exhibited large fluctuations, from 1.4 to 55.2 μg/m^3 (mean value: 10.1 ± 10.5 μg/m^3). The aerosol pH values of $PM_{2.5}$ in Kunming were much higher than those in the US (Guo et al., 2015, 2016, 2017a), but lower than those reported in several previous studies. For example, the pH of $PM_{2.5}$ in northern China during severe haze episodes was reported to be
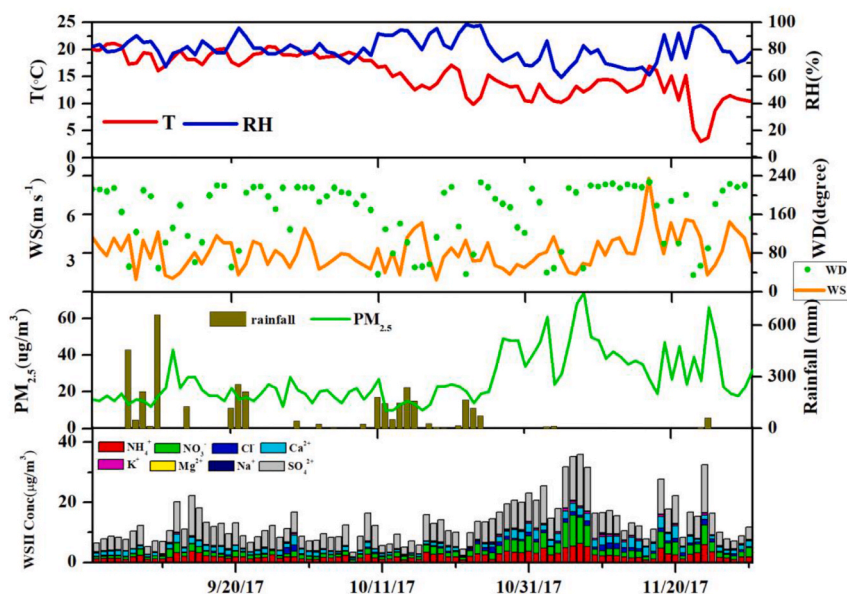
Fig. 1. Meteorological conditions including T, RH, wind speed-WS, wind direction-WD and rainfall (mm), mass concentrations of $PM_{2.5}$ and water soluble inorganic ions (WSIIs) during the autumn of 2017.
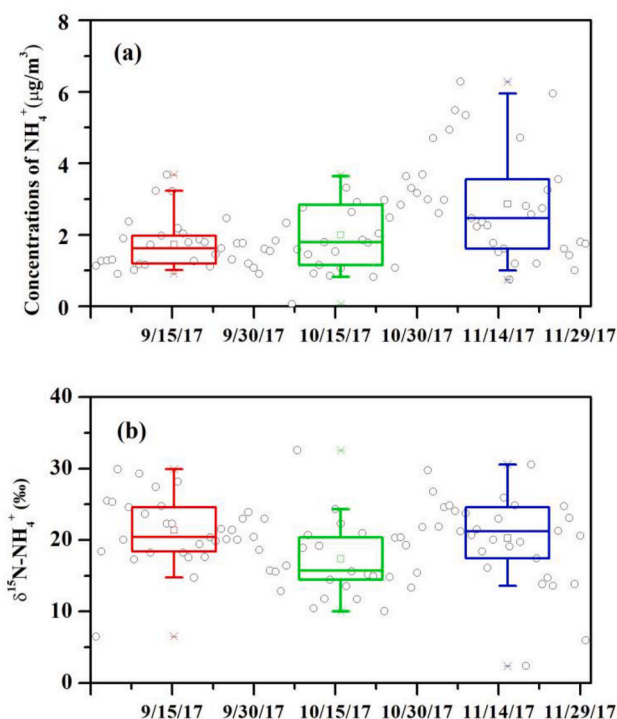

Fig. 2. (a) Daily concentrations of particulate NH_4^+ and (b) daily $\delta^{15}N–NH_4^+$ values in the autumn of 2017.

between 3.0 and 4.9 (Liu et al., 2017), while in rural Europe was 3.7 (Guo et al., 2018). The average pH of PM_3 in urban Guangzhou was reported to be between 2.6 and 5.6 (Jiang et al., 2019). Aerosol acidity or pH is one of the most important properties in aerosol chemistry processes, which affects the gas-particle partitioning of semi-volatile or volatile species like $NH_3–NH_4^+$.

3.1.3. The $\delta^{15}N$ value of NH_4^+ in $PM_{2.5}$

The $\delta^{15}N$ values of NH_4^+ in $PM_{2.5}$ over the sampling autumn season varied remarkably from −6.4‰ to 32.5‰, with an average value of 19.2

± 6.4‰ (Fig. 2). These $\delta^{15}N$ values fell within the wide range of previous $\delta^{15}N–NH_4^+$ measurements reported in Korea (4.3 to +23.6‰ and −25.6 to +21.8‰ in Seoul and Baengnyeong Island, respectively Park et al. (2018)) and in urban cities of northern China and central China in the autumn of 2017 (Beijing: 33.2 to +35.6‰, Tianjing: +1.9‰ to +30‰, Shijiazhuang: 17.2 to +32.9‰ (Zhang et al., 2020b); Nanchang: −3.2‰ to +24.2‰, Wuhan: +3.0‰ to +36.4‰, Changsha: +1.0‰ to +29.2‰ (Xiao et al., 2020)). These $\delta^{15}N–NH_4^+$ values were significantly higher than those reported both in the summer and winter of Beijing in 2013 (−11 to +5.9‰, −39 to +5‰, Pan et al. (2018b); Pan et al. (2016)), the south Atlantic ocean (−13 to +15‰, Lin et al. (2016)), and northeastern Alberta, Canada (−4.5 to +20.1‰, Proemse et al. (2012)), but the average $\delta^{15}N–NH_4^+$ value was slightly lower than that recorded in downtown Toronto, Canada (+23.6‰, Smirnoff et al. (2012)). Previously mentioned $\delta^{15}N–NH_4^+$ in $PM_{2.5}$ over the world were listed in Table S2. Monthly average values of $\delta^{15}N–NH_4^+$ were 21.3 ± 4.6‰, 16.1 ± 7.1‰ and 20.2 ± 6.1‰, respectively (Fig. 2). The value of $\delta^{15}N–NH_4^+$ was not showed significantly correlations with NH_4^+ concentration, which implied shifty sources of ambient ammonia or various degrees of ammonia gas-particle conversion ratio (*f*) from month to month.

If the isotopic effect between ambient NH_3 and particulate NH_4^+ is not taken into consideration, the $\delta^{15}N$ value of NH_4^+ measured in $PM_{2.5}$ can directly represents $\delta^{15}N–NH_3$ in the atmosphere. However, the $\delta^{15}N–NH_4^+$ values of $PM_{2.5}$ in this study were obviously fell beyond the range of $\delta^{15}N–NH_3$ values of various sources (−50 ± 1.8‰ to +12‰, Chang et al. (2016a); Kawashima and Kurahashi (2011)), suggesting that it was impossible for particulate NH_4^+ to be formed directly by the mixing of gas ammonia that emitted from different sources without isotopic fractionation during ammonia gas-particle conversion process. In previous studies, the $\delta^{15}N$ values of NH_3 in the atmosphere fell within a more negative range compared to the $\delta^{15}N$ values of particulate NH_4^+ (Tables S1 and S2). ^{15}N isotope relatively enriched in particulate phase when isotopic effect occurred during the gas-particle conversion process. The compilation of previous studies from Chang et al. (2019a) revealed that ^{15}N in particulate NH_4^+ is more enriched than NH_3 by 23‰ on average.

3.2. The self-amplifying loop

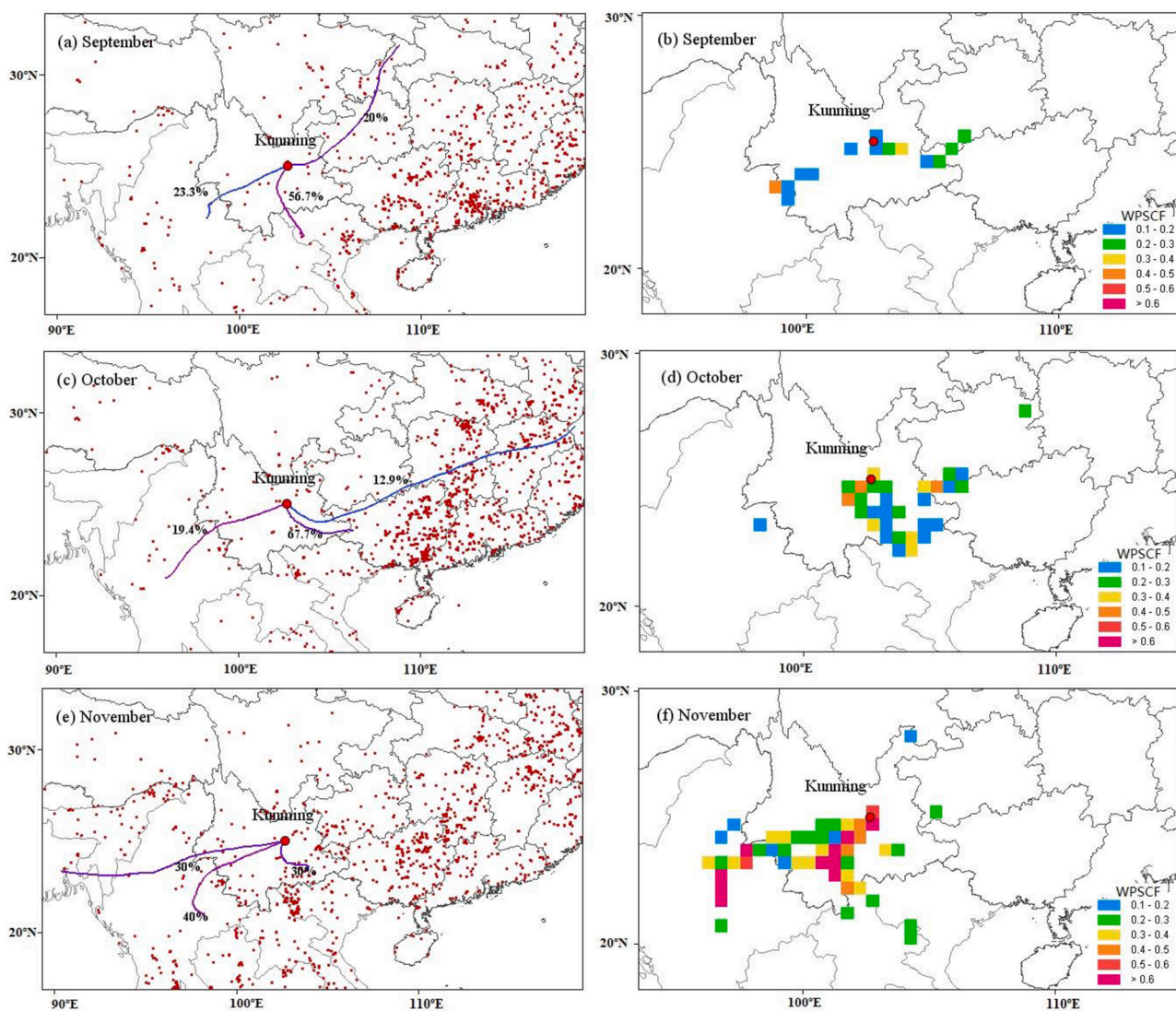In order to further explore the relationships between the chemical

Fig. 3. Back-trajectories clustering results for every month of autumn in 2017 with the geographical distribution of fire spots (obtained from http://firefly.geog.umd. edu/fire map/). Map of potential source regions of NH_4^+ in $PM_{2.5}$. WPSCF values were in direct proportion to the potential of NH_3 emission sources.

composition and property when particulate NH_4^+ concentration elevated (Fig. 1), the data of November were selected for discussion. On the one hand, the concentration of $PM_{2.5}$ and chemical compositions were significantly increased in November when several slightly polluted periods occurred. On the other hand, precipitation was frequent in September and October and rainfall events greatly affected aerosol liquid water content, which might interfere with the result.

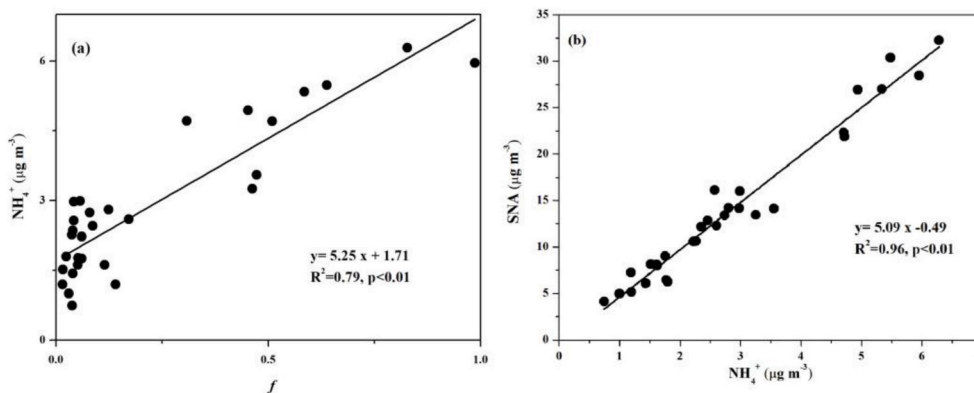The ammonia gas-particle conversion ratio (f) is defined as the molar

Fig. 4. (a) The concentration of NH_4^+ as a function of ammonia gas-particle conversion ratio (f), (b) the concentration of SNA as a function of the concentration of NH_4^+.

ratio between particulate ammonium and total ammonia (Equation (8)). The ammonia gas-particle conversion ratio (f) in this study was calculated based on the formula provided in Section 2.5. The particulate NH_4^+ mass concentration was determined by the initial concentration of ambient ammonia and f. A recent study conducted in downtown Shanghai found that the SNA (sulfate, nitrate and ammonium) mass concentration in $PM_{2.5}$ was linearly correlated with the gas-particle conversion ratio (f), where a higher NH_3 concentration promoted the strong formation of SNA (Xu et al., 2020a). However, in this study, particulate NH_4^+ mass concentration showed a linear increase with the increase of f (Fig. 4a, $R^2 = 0.79$, p < 0.01), which indicated that the concentration of initial ambient ammonia might be decreased when NH_4^+ levels elevated in Kunming during the late autumn. The concentrations of ambient ammonia in southwest China were relatively lower compared to other cities in Northern China Plain (Kong et al., 2019). During haze periods, with increases in $PM_{2.5}$ levels, SNA mass concentrations exhibited explosive growth pattern (Huang et al., 2014; Wang et al., 2016). An increase in ammonium salt concentrations was associated with an increase in nitrate and sulfate concentrations, in this study, a good linear relationship was observed between the concentrations of SNA and ammonium salt (Fig. 4b, $R^2 = 0.96$, p < 0.01). Previous studies have mentioned that aerosol pH can be influenced by chemical compositions and environmental factors, such as environmental temperature, relative humidity, aerosol liquid water content, and even gas precursors like ammonia (Guo et al., 2017b; Liu et al., 2017; Wang et al., 2020).

It has been reported that a substantial fraction of ALWC was mainly driven by anthropogenic sulfate or nitrate in many previous studies (Carlton and Turpin, 2013; Guo et al., 2015; Nguyen et al., 2016; Xu et al., 2020b). Further, the ALWC over the Italian Po Valley and NCP of China were controlled by anthropogenic nitrate (Hodas et al., 2014; Wu et al., 2018). Recently, a long-term observation in Beijing have revealed that ALWC ranged from 2% up to 74% while the secondary inorganic salt fraction elevated from 24% to 55% and the ambient relative humidity increased from 15% to 83% (Wu et al., 2018). In this study, the fraction of ALWC showed exponential growth with the increasing SNA mass concentrations (Fig. 5a, $R^2 = 0.59$, p < 0.01), while it was poorly correlated with RH, mainly due to the narrow range of RH values. Wu et al. (2018) proposed a hypothesis to explain why ALWC is driven by SNA concentration. Accordingly, increasing anthropogenic emissions of polluted gas (SO_2 and NO_2) will constantly partition into the condensed phase following Henry's law, which induces depletion of species between gas and condensed phase, leading to water uptake to balance this depletion. Further, according to the gas-liquid equilibrium of $NH_3(g)$-NH_4^+(aq, s) system, elevated hydrogen ions facilitate the equilibrium toward the particle phase when aerosol pH is decreased. In the current study, aerosol pH was positively correlated with SNA mass concentrations (Fig. 5b, $R^2 = 0.57$, p < 0.01).

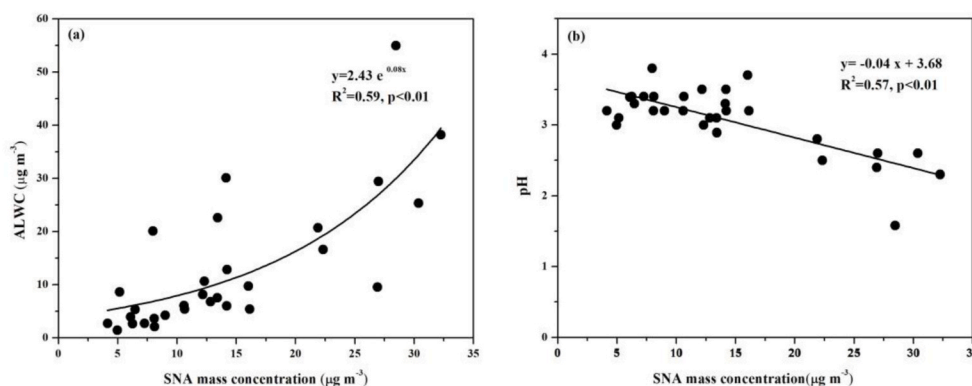According to the computational formula, the ammonia gas-particle

conversion ratio (f) is controlled by T, pH, ALWC, and $\frac{\gamma_{(H^+)}}{\gamma_{(NH_4^+)}}$. It increases with the decreases in T and pH, and increases in ALWC and $\frac{\gamma_{(H^+)}}{\gamma_{(NH_4^+)}}$. In general, a low ammonia conversion ratio, which is usually observed in summer, is attributed to the preference of particulate ammonium to convert into the gas phase when the relative equilibrium condition is approached under relative rich environment of ambient NH_3 with higher T. Likewise, ammonium tends to be preserved in particle phase under lower T, resulting in much higher f. An improved inversion estimation of NH_3 emissions in China has been employed to reconstruct a more distinct seasonality, with emissions in summer being twice as those in winter (Kong et al., 2019). Under a rich environment of atmospheric NH_3 during the warm season, more significant isotopic fractionation could be anticipated in the urban atmospheres, as compared to during cold season (Pan et al., 2018b; Wang et al., 2017). In this study, f was poorly correlated with T and $\frac{\gamma_{(H^+)}}{\gamma_{(NH_4^+)}}$ due to the relatively narrow range of T and $\frac{\gamma_{(H^+)}}{\gamma_{(NH_4^+)}}$ values in late autumn in the study area. However, as can be seen in Fig. 6, the ammonia gas-particle conversion ratio (f) was positive correlated with ALWC mass concentrations and increased with the decreasing pH. This indicated that these parameters (pH and ALWC) mainly regulate the ammonia convert ratio in late
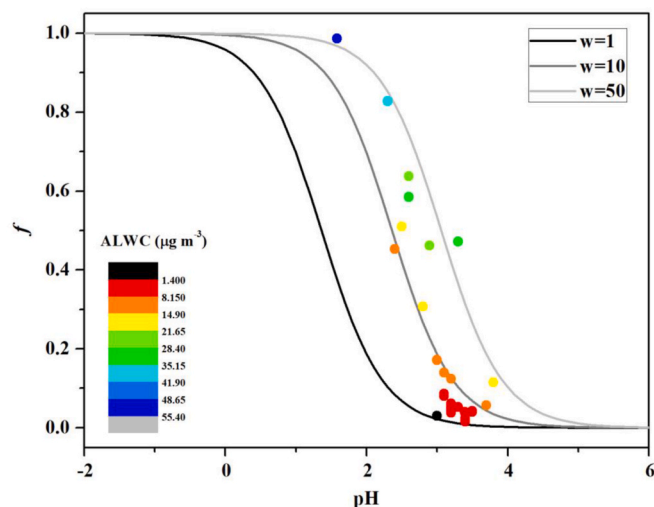

Fig. 6. Analytically calculated S curve of the ammonia gas-particle conversion ratio (f) plotted with ISORROPIA-II predicted pH based on different aerosol liquid water content (w = 1, w = 10 and w = 50 μg/m³) and average temperature, the solid points represent the daily f plotted with ISORROPIA-predicted pH from meteorological data and concentrations of $PM_{2.5}$ in late autumn in Kunming.

Fig. 5. (a) ALWC and (b) aerosol pH as a function of the concentration of SNA.

autumn in Kunming. A recent study reported that ALWC was the key factor in the ammonia gas-particle conversion ratio rather than T, pH, and $\frac{\gamma_{(H^+)}}{\gamma_{(NH_4^+)}}$ in the rural agricultural environment in Shanghai (Xu et al., 2020a).

Based on the discussion above, a possible self-amplifying feedback loop in Kunming was proposed when ammonium salt mass concentrations in $PM_{2.5}$ were increased. In brief, the substantial gas-particle conversion of NH_4^+ was initiated with remarkable increases in SNA. Further, an increase in sulfate and nitrate concentrations, in step with the increase of ammonium concentrations, would lead to a decrease in the pH of $PM_{2.5}$. Elevated SNA enhanced water uptake via particle hygroscopic properties to maintain thermodynamic equilibrium. The increased ALWC and decreased pH facilitated the ammonia gas-particle conversion efficiency and then formed more ammonium salt, thus triggering the feedback mechanism. Then more particulate NH_4^+ and other SNA were further formed.

3.3. Source apportionment of ambient ammonia

Since the isotopic effect exists during the ammonia gas-particle conversion process, the $\delta^{15}N$ values of NH_4^+ in $PM_{2.5}$ cannot be directly used to trace ambient NH_3 emissions. The potential isotopic fractionation between ambient NH_3 and particulate NH_4^+, which can be estimated based on Section 2.4, is the key to calculating the $\delta^{15}N$ value of ambient NH_3. According to Equation (1), the predicted $\delta^{15}N$–NH_3 values varied from −27.4‰ to 15.3‰, with an average of −8.1 ± 8.3‰. Monthly concentration-weighted mean ^{15}N–NH_3 values were −6.7‰, −9.6‰ and −1.6‰ in September, October and November, respectively. These $\delta^{15}N$–NH_3 values fell within the wide range of $\delta^{15}N$–NH_3 values reported in previous studies (Table S1) and the average value was slightly higher than those measured in the rural Moravia-Silesian region, Czech Republic, in summer (−10.3 ± 12.5‰, Buzek et al. (2017)), urban Colorado, US (−10.0 ± 2.6‰ (clean air), Moore (1977)), Taihu Lake of China (−16.7, −18.2‰ and −17.4‰, Ti et al. (2018)), the US (−15.1 ± 9.7‰, Felix et al. (2017), −19.1 ± 12.7‰, Berner and Felix (2020)), Guiyang, China (−16.8 ± 4.9‰, Xiao et al. (2015)), and significantly higher than those reported for Shanghai (−31.7 ± 3.3‰, Chang et al. (2019b)), the rural Moravia-Silesian region, Czech Republic, in winter (−24.8 ± 15.4‰, Buzek et al. (2017)), and urban Beijing, China (−35.3 ± 5.4‰, Chang et al. (2016a)). The relatively high $\delta^{15}N$–NH_3 values in Kunming implied that more NH_3 was related to non-agricultural emissions (including fossil fuel combustion and biomass burning).

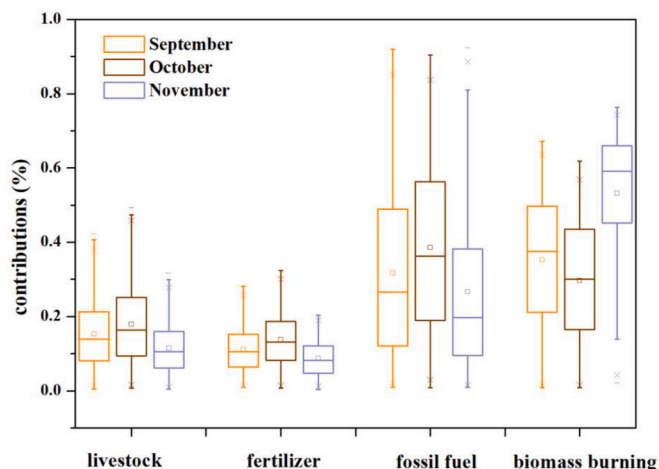Once the $\delta^{15}N$ value of initial NH_3 was calculated based on the ammonia gas-to-particle partitioning process, the isotopic mixing model was then performed to apportion the contributions of ambient NH_3 sources. As illustrated in Fig. 7, ambient NH_3 emitted from agricultural sources (livestock and fertilizer; 20.1%–31.6%) and non-agricultural sources (fossil fuel combustion and biomass burning; 68.3%–79.8%) collectively influenced the ambient NH_3 in Kunming. And non-agricultural emissions dominated ambient NH_3 levels in this plateau city in the autumn of 2017. Interestingly, it could be obviously noticed that the contributions of biomass burning emissions were significantly enhanced from 35 ± 17.1% in September and 29.7 ± 15.6% in October to 53.2 ± 17% in November, while ammonium levels significantly elevated in this month. From the above discussion (Section 3.1.1), ambient ammonia in November from biomass burning emissions might have been originated from local emissions and regional transport process in late autumn when PSCF analysis identified the dominant source areas in Burma, southwest Yunnan province and the local areas of Kunming in November (Fig. 2). In central China, biomass burning emissions dominated ambient ammonia in November, however, wild fire showed minimal potential to influence biomass burning emissions, while increase use of biomass fuel in the residential sector lead to NH_4^+ levels elevated (Xiao et al., 2020). But indoor biofuel burning for household cooking and heating could not be detected by satellite. Biofuel was one of the most important energy sources of Yunnan Province, ranking the top three in China in terms of reservoir potential and yield (Liu and Shen, 2007). Daily contributions of different sources in November were shown in Fig. 8, in clean periods, biomass burning emissions accounted for 12.4%–45.2% of ambient ammonia (average contribution of 28.4%), while in polluted periods, the contributions of biomass burning showed a significant increase and elevated up to 44.8%–99.1% (average contribution of 76.5%). It could be inferred from Fig. 8 that biomass burning emissions might play a key role during slightly polluted days in Kunming, which was similar to what was found in central China (Xiao et al., 2020). In addition, it could also be found that the concentrations of NH_4^+ from biomass burning source showed well correlation with NH_4^+ concentrations in $PM_{2.5}$ (R^2 = 0.94, p < 0.01, Fig. 9). Ambient NH_3 from biomass burning emissions gradually occupied vital proportions with increasing NH_4^+ concentrations in the autumn of 2017 in Kunming. When the concentrations of NH_4^+ exceeded 5.0 μg/m³, almost all of the ambient ammonia originated from biomass burning emissions (Fig. 9). Differently, previous studies have reported that fossil fuel combustion-related emissions dominated atmospheric ammonia sources during severe haze episodes in northern China
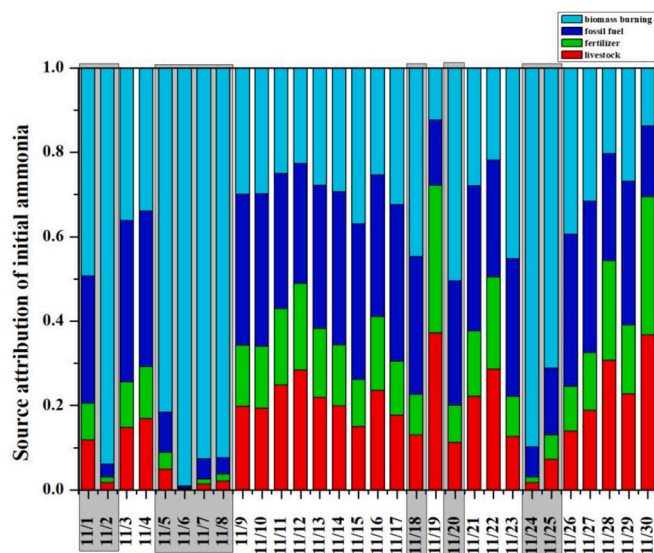

Fig. 7. Monthly contributions of emissions from different sources to ambient NH_3 concentrations in autumn in Kunming.

Fig. 8. Daily contributions of emissions from different sources to ambient NH_3 concentrations in November in Kunming; the slightly polluted periods are sighed by the shadow.
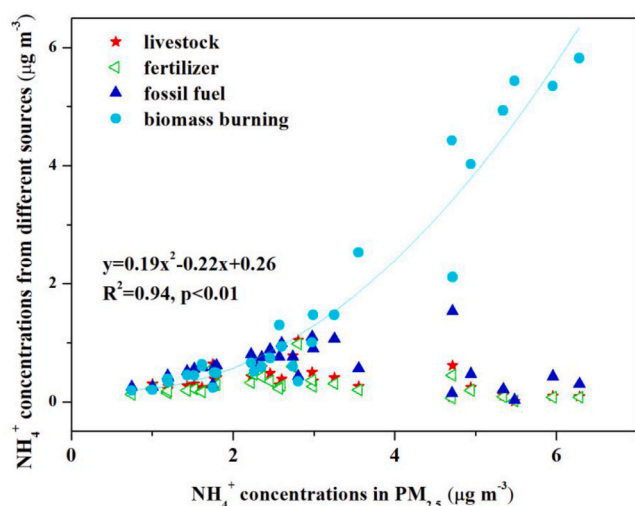
Fig. 9. NH_4^+ compositions from four different sources at different NH_4^+ concentrations. Natural index relationship between NH_4^+ concentrations from biomass burning and total NH_4^+ concentrations in $PM_{2.5}$.

megacities (Pan et al., 2016; Zhang et al., 2020b). This study provide valid approach to ammonia source apportionment, however, a large of uncertainties were raised due to limit acknowledge of the $\delta^{15}N–NH_3$ values of ammonia sources, especially for the nitrogen composition of biomass burning (only one $\delta^{15}N–NH_3$ value of biomass burning emissions was recorded in previous study, Kawashima and Kurahashi (2011)). Therefore, it is necessary to further conduct systematic study to accurately investigate the nitrogen isotopic compositions of each source of atmospheric ammonia.

In general, ambient ammonia during slightly polluted days was mainly dominated by biomass burning emissions, which might have been originated from local emissions and regional transport process in late autumn. And enhanced biomass burning related ammonia emissions promoted a self-amplifying loop for particulate NH_4^+ formation in late autumn. The results of this study may not only shed light on the sources and processes of atmospheric ammonia, but may also give insight into relevant government policies and regulations to improve air quality in Kunming.

4. Conclusions

This study mainly focused on the concentrations and the nitrogen isotopic compositions of aerosol NH_4^+ in autumn in a typical southwest plateau city, Kunming. During this transition season, the average concentrations of aerosol NH_4^+ were 1.7 ± 0.6 μg/m³, 1.9 ± 0.9 μg/m³, and 2.8 ± 1.5 μg/m³ in September, October, and November, respectively; concentrations showed sustained growth and were significantly elevated in November. The $\delta^{15}N$ values of NH_4^+ in $PM_{2.5}$ over the sampling period varied remarkably from -6.4‰ to 32.5‰, with an average of 19.2 ± 6.4‰.

Since the nitrogen isotopic effect between ambient NH_3 and particulate NH_4^+ was taken into consideration, the ISORROPIA-II model was run to obtain the aerosol pH and aerosol liquid water content (ALWC). Then, the ammonia gas-particle conversion ratio (f) was calculated for each day in November. Based on the inverse analysis of the nitrogen isotopic composition of particulate NH_4^+, the initial $\delta^{15}N$ values of ambient NH_3 were estimated to be -27.4‰–15.3‰, with an average of -8.1 ± 8.3‰.

Based on the findings of this study, we proposed a self-amplifying feedback mechanism of NH_4^+ formation associated with ALWC concentration, pH, and the ammonia gas-particle conversion ratio (f) in Kunming.

Further, isotope-based source apportionment of NH_3 in Kunming

illustrated that biomass burning sources dominated the ambient NH_3 during slightly polluted days. Back trajectories derived from southeast Asia contributed to 70% of the total trajectories, and it could be noticed from fire maps that fire spots distributed around Kunming city and Southeast Asia were evidently concentrated in November. PSCF analysis revealed that the concentrations of aerosol NH_4^+ were influenced by regional and local areas in November. In general, ambient NH_3 during polluted days was dominated by biomass burning emissions, which might have been originated from local emissions and regional transport process in late autumn.

CRediT authorship contribution statement

Yunhong Zhou: Methodology, Data curation, Writing - original draft. **Nengjian Zheng:** Methodology, Supervision, Writing - review & editing. **Li Luo:** Data curation. **Jingjing Zhao:** Visualization. **Linglu Qu:** Visualization. **Hui Guan:** Data curation, Investigation. **Hongwei Xiao:** Visualization. **Zhongyi Zhang:** Data curation. **Jing Tian:** Visualization. **Huayun Xiao:** Conceptualization, Methodology, Supervision, Writing - review & editing.

Declaration of competing interest

The authors declare that they have no known competing financial interests or personal relationships that could have appeared to influence the work reported in this paper.

Acknowledgments

Appendix A. Supplementary data

Supplementary data to this article can be found online at https://doi.org/10.1016/j.atmosenv.2020.118138.

References

Almeida, S.M., Lage, J., Fernandez, B., Garcia, S., Reis, M.A., Chaves, P.C., 2015. Chemical characterization of atmospheric particles and source apportionment in the vicinity of a steelmaking industry. Sci. Total Environ. 521–522, 411–420.

Berner, A.H., Felix, J.D., 2020. Investigating ammonia emissions in a coastal urban airshed using stable isotope techniques. Sci. Total Environ. 707, 13.

Buzek, F., Cejkova, B., Hellebrandova, L., Jackova, I., Lollek, V., Lnenickova, Z., et al., 2017. Isotope composition of NH_3, NOx and SO_2 air pollution in the Moravia-Silesian region, Czech Republic. Atmos. Pollut. Res. 8 (2), 221–232.

Carlton, A.G., Turpin, B.J., 2013. Particle partitioning potential of organic compounds is highest in the Eastern US and driven by anthropogenic water. Atmos. Chem. Phys. 13 (20), 10203–10214.

Chang, Y.H., Liu, X.J., Deng, C.R., Dore, A.J., Zhuang, G.S., 2016a. Source apportionment of atmospheric ammonia before, during, and after the 2014 APEC summit in Beijing using stable nitrogen isotope signatures. Atmos. Chem. Phys. 16 (18), 11635–11647.

Chang, Y.H., Zhang, Y.L., Li, J.R., Tian, C.G., Song, L.L., Zhai, X.Y., et al., 2019a. Isotopic constraints on the atmospheric sources and formation of nitrogenous species in clouds influenced by biomass burning. Atmos. Chem. Phys. 19 (19), 12221–12234.

Chang, Y.H., Zou, Z., Deng, C.R., Huang, K., Collett, J.L., Lin, J., et al., 2016b. The importance of vehicle emissions as a source of atmospheric ammonia in the megacity of Shanghai. Atmos. Chem. Phys. 16 (5), 3577–3594.

Chang, Y.H., Zou, Z., Zhang, Y.L., Deng, C.R., Hu, J.L., Shi, Z.H., et al., 2019b. Assessing contributions of agricultural and nonagricultural emissions to atmospheric ammonia in a Chinese megacity. Environ. Sci. Technol. 53 (4), 1822–1833.

Davis, P., Syme, J., Heikoop, J., Fessenden-Rahn, J., Perkins, G., Newman, B., et al., 2015. Quantifying uncertainty in stable isotope mixing models. J. Geophys. Res. Biogeosci. 120 (5), 903–923.

Felix, J.D., Elliott, E.M., Gay, D.A., 2017. Spatial and temporal patterns of nitrogen isotopic composition of ammonia at US ammonia monitoring network sites. Atmos. Environ. 150, 434–442.

Felix, J.D., Elliott, E.M., Gish, T.J., McConnell, L.L., Shaw, S.L., 2013. Characterizing the isotopic composition of atmospheric ammonia emission sources using passive

samplers and a combined oxidation-bacterial denitrifier approach. Rapid Commun. Mass Spectrom. 27 (20), 2239–2246.

Fountoukis, C., Nenes, A., 2007. Isorropia II: a computationally efficient thermodynamic equilibrium model for K^+-Ca^{2+}-Mg^{2+}-NH_4^+-Na^+-SO_4^{2-}-NO_3^--Cl^--H_2O aerosols. Atmos. Chem. Phys. 7 (17), 4639–4659.

Freyer, H.D., 1978. Seasonal trends of NH_4^+ and NO_3^- nitrogen isotope composition in rain collected at julich, Germany. Tellus 30 (1), 83–92.

Guo, H.Y., Liu, J.M., Froyd, K.D., Roberts, J.M., Veres, P.R., Hayes, P.L., et al., 2017a. Fine particle pH and gas-particle phase partitioning of inorganic species in Pasadena, California, during the 2010 CalNex campaign. Atmos. Chem. Phys. 17 (9), 5703–5719.

Guo, H.Y., Otjes, R., Schlag, P., Kiendler-Scharr, A., Nenes, A., Weber, R.J., 2018. Effectiveness of ammonia reduction on control of fine particle nitrate. Atmos. Chem. Phys. 18 (16), 12241–12256.

Guo, H.Y., Sullivan, A.P., Campuzano-Jost, P., Schroder, J.C., Lopez-Hilfiker, F.D., Dibb, J.E., et al., 2016. Fine particle pH and the partitioning of nitric acid during winter in the northeastern United States. J. Geophys. Res. Atmos. 121 (17), 10355–10376.

Guo, H.Y., Weber, R.J., Nenes, A., 2017b. High levels of ammonia do not raise fine particle pH sufficiently to yield nitrogen oxide-dominated sulfate production. Sci. Rep. 7 (1), 12109.

Guo, H.Y., Xu, L., Bougiatioti, A., Cerully, K.M., Capps, S.L., Hite, J.R., et al., 2015. Fine-particle water and pH in the southeastern United States. Atmos. Chem. Phys. 15 (9), 5211–5228.

Heaton, T.H.E., Spiro, B., Madeline, S., Robertson, C., 1997. Potential canopy influences on the isotopic composition of nitrogen and sulphur in atmospheric deposition. Oecologia 109 (4), 600–607.

Hodas, N., Sullivan, A.P., Skog, K., Keutsch, F.N., Collett, J.L., Decesari, S., et al., 2014. Aerosol liquid water driven by anthropogenic nitrate: implications for lifetimes of water-soluble organic gases and potential for secondary organic aerosol formation. Environ. Sci. Technol. 48 (19), 11127–11136.

Huang, R.J., Zhang, Y.L., Bozzetti, C., Ho, K.F., Cao, J.J., Han, Y.M., et al., 2014. High secondary aerosol contribution to particulate pollution during haze events in China. Nature 514 (7521), 218–222.

Huang, X., Song, Y., Li, M., Li, J., Huo, Q., Cai, X., et al., 2012. A high-resolution ammonia emission inventory in China. Global Biogeochem. Cycles 26 (1).

Jiang, F., Liu, F.X., Lin, Q.H., Fu, Y.Z., Yang, Y.X., Peng, L., et al., 2019. Characteristics and formation mechanisms of sulfate and nitrate in size-segregated atmospheric particles from urban Guangzhou, China. Aerosol. Air Qual. Res. 19 (6), 1284–1293.

Kang, Y.N., Liu, M.X., Song, Y., Huang, X., Yao, H., Cai, X.H., et al., 2016. High-resolution ammonia emissions inventories in China from 1980 to 2012. Atmos. Chem. Phys. 16 (4), 2043–2058.

Kawashima, H., Kurahashi, T., 2011. Inorganic ion and nitrogen isotopic compositions of atmospheric aerosols at Yurihonjo, Japan: implications for nitrogen sources. Atmos. Environ. 45 (35), 6309–6316.

Kirshenbaum, I., Smith, J.S., Crowell, T., Graff, J., McKee, R., 1947. Separation of the nitrogen isotopics by the exchange reaction between ammonia and solutions of ammonium nitrate. J. Chem. Phys. 15 (7), 440–446.

Kong, L., Tang, X., Zhu, J., Wang, Z.F., Pan, Y.P., Wu, H.J., et al., 2019. Improved inversion of monthly ammonia emissions in China based on the Chinese ammonia monitoring network and ensemble kalman filter. Environ. Sci. Technol. 53 (21), 12529–12538.

Lin, C.T., Jickells, T.D., Baker, A.R., Marca, A., Johnson, M.T., 2016. Aerosol isotopic ammonium signatures over the remote Atlantic Ocean. Atmos. Environ. 133, 165–169.

Liu, B.S., Song, N., Dai, Q.L., Mei, R.B., Sui, B.H., Bi, X.H., et al., 2016. Chemical composition and source apportionment of ambient $PM_{2.5}$ during the non-heating period in Taian, China. Atmos. Res. 170, 23–33.

Liu, G., Shen, L., 2007. Quantitive appraisal of biomass energy and its geographical distribution in China. J. Nat. Resour. 22 (1), 9–19.

Liu, L., Guo, J.P., Miao, Y.C., Liu, L., Li, J., Chen, D.D., et al., 2018. Elucidating the relationship between aerosol concentration and summertime boundary layer structure in central China. Environ. Pollut. 241, 646–653.

Liu, M., Huang, X., Song, Y., 2019. Ammonia emission control in China would mitigate_ haze pollution and nitrogen deposition, but worsen acid rain. Proc. Natl. Acad. Sci. Unit. States Am. 116.

Liu, M.X., Song, Y., Zhou, T., Xu, Z.Y., Yan, C.Q., Zheng, M., et al., 2017. Fine particle pH during severe haze episodes in northern China. Geophys. Res. Lett. 44 (10), 5213–5221.

Lou, M.Y., Guo, J.P., Wang, L.L., Xu, H., Chen, D.D., Miao, Y.C., et al., 2019. On the relationship between aerosol and boundary layer height in summer in China under different thermodynamic conditions. Earth Space Sci. 6 (5), 887–901.

Moore, H., 1977. The isotopic composition of ammonia, nitrogen dioxide and nitrate in the atmosphere. Atmos. Environ. 11 (12), 1239–1243, 1967.

Nguyen, T.K.V., Zhang, Q., Jimenez, J.L., Pike, M., Carlton, A.G., 2016. Liquid water: ubiquitous contributor to aerosol mass. Environ. Sci. Technol. Lett. 3 (7), 257–263.

Pan, Y.P., Tian, S.L., Liu, D.W., Fang, Y.T., Zhu, X., Gao, M., et al., 2018a. Isotopic evidence for enhanced fossil fuel sources of aerosol ammonium in the urban atmosphere. Environ. Pollut. 238, 942–947.

Pan, Y.P., Tian, S.L., Liu, D.W., Fang, Y.T., Zhu, X.Y., Gao, M., et al., 2018b. Source apportionment of aerosol ammonium in an ammonia-rich atmosphere: an isotopic study of summer clean and hazy days in urban beijing. J. Geophys. Res. Atmos. 123 (10), 5681–5689.

Pan, Y.P., Tian, S.L., Liu, D.W., Fang, Y.T., Zhu, X.Y., Zhang, Q., et al., 2016. Fossil fuel combustion-related emissions dominate atmospheric ammonia sources during severe haze episodes: evidence from ^{15}N-stable isotope in size-resolved aerosol ammonium. Environ. Sci. Technol. 50 (15), 8049–8056.

Park, Y.M., Park, K.S., Kim, H., Yu, S.M., Noh, S., Kim, M.S., et al., 2018. Characterizing isotopic compositions of TC-C, NO_3-N, and NH_4^+-N in $PM_{2.5}$ in South Korea: impact of China's winter heating. Environ. Pollut. 233, 735–744.

Polissar, A.V., Hopke, P.K., Paatero, P., Kaufmann, Y.J., Hall, D.K., Bodhaine, B.A., et al., 1999. The aerosol at Barrow, Alaska: long-term trends and source locations. Atmos. Environ. 33 (16), 2441–2458.

Proemse, B.C., Mayer, B., Chow, J.C., Watson, J.G., 2012. Isotopic characterization of nitrate, ammonium and sulfate in stack $PM_{2.5}$ emissions in the Athabasca Oil Sands Region, Alberta, Canada. Atmos. Environ. 60, 555–563.

Seinfeld, J.H., Pandis, S.N., Noone, K., 2006. Atmospheric Chemistry and Physics: from Air Pollution to Climate Change.

Smirnoff, A., Savard, M.M., Vet, R., Simard, M.C., 2012. Nitrogen and triple oxygen isotopes in near-road air samples using chemical conversion and thermal decomposition. Rapid Commun. Mass Spectrom. 26 (23), 2791–2804.

Su, T.N., Li, Z.Q., Zheng, Y.T., Luan, Q.Z., Guo, J.P., 2020. Abnormally shallow boundary layer associated with severe air pollution during the COVID-19 lockdown in China. Geophys. Res. Lett., e2020GL090041

Ti, C.P., Gao, B., Luo, Y.X., Wang, X., Wang, S.W., Yan, X.Y., 2018. Isotopic characterization of NHx-N in deposition and major emission sources. Biogeochemistry 138 (1), 85–102.

Wang, S.B., Wang, L.L., Li, Y.Q., Wang, C., Wang, W.S., Yin, S.S., et al., 2020. Role of ammonia on fine-particle pH in agricultural regions of China: comparison between urban and rural sites. Atmos. Chem. Phys. 20 (5), 2719–2734.

Wang, G.H., Zhang, R.Y., Gomez, M.E., Yang, L.X., Zamora, M.L., Hu, M., et al., 2016. Persistent sulfate formation from London Fog to Chinese haze. Proc. Natl. Acad. Sci. U. S. A. 113 (48), 13630–13635.

Wang, Y.L., Liu, X.Y., Song, W., Yang, W., Han, B., Dou, X.Y., et al., 2017. Source appointment of nitrogen in $PM_{2.5}$ based on bulk delta ^{15}N signatures and a Bayesian isotope mixing model. Tellus Ser. B Chem. Phys. Meteorol. 69, 10.

Wu, S.P., Zhu, H., Liu, Z., Dai, L.H., Zhang, N., Schwab, J.J., et al., 2019. Nitrogen isotope composition of ammonium in PM2.5 in the Xiamen, China: impact of non-agricultural ammonia. Environ. Sci. Pollut. Control Ser. 26 (25), 25596–25608.

Wu, Z.J., Wang, Y., Tan, T.Y., Zhu, Y.S., Li, M.R., Shang, D.J., et al., 2018. Aerosol liquid water driven by anthropogenic inorganic salts: implying its key role in haze formation over the north China plain. Environ. Sci. Technol. Lett. 5 (3), 160–166.

Xiao, H.-W., Wu, J.-F., Luo, L., Liu, C., Xie, Y.-J., Xiao, H.-Y., 2020. Enhanced biomass burning as a source of aerosol ammonium over cities in Central China in autumn. Environ. Pollut. 115278.

Xiao, H.W., Xiao, H.Y., Long, A.M., Liu, C.Q., 2015. Delta ^{15}N-NH4+ variations of rainwater: application of the Rayleigh model. Atmos. Res. 157, 49–55.

Xu, J., Chen, J., Zhao, N., Wang, G., Yu, G., Li, H., et al., 2020a. Importance of ammonia gas-particle conversion ratio in haze formation in the rural agricultural environment. Atmos. Chem. Phys. 20 (12), 7259–7269.

Xu, Y., Miyazaki, Y., Tachibana, E., Sato, K., Ramasamy, S., Mochizuki, T., et al., 2020b. Aerosol liquid water promotes the formation of water-soluble organic nitrogen in submicrometer aerosols in a suburban forest. ES T (Environ. Sci. Technol.) 54 (3), 1406–1414.

Yin, D.Y., Zhao, S.P., Qu, J.J., 2017. Spatial and seasonal variations of gaseous and particulate matter pollutants in 31 provincial capital cities, China. Air Qual. Atmos. Health 10 (3), 359–370.

Zhang, F., Cheng, H.R., Wang, Z.W., Lv, X.P., Zhu, Z.M., Zhang, G., et al., 2014. Fine particles ($PM_{2.5}$) at a CAWNET background site in Central China: chemical compositions, seasonal variations and regional pollution events. Atmos. Environ. 86, 193–202.

Zhang, L., Altabet, M.A., Wu, T.X., Hadas, O., 2007. Sensitive measurement of (NH4+N)-N-15/N-14 (delta(NH4+)-N-15) at natural abundance levels in fresh and saltwaters. Anal. Chem. 79 (14), 5297–5303.

Zhang, Y., Guo, J.P., Yang, Y.J., Wang, Y., Yim, S.H., 2020a. Vertical wind shear modulates particulate matter pollution: a perspective from radar wind profiler observations in beijing, China. Rem. Sens. 12, 546.

Zhang, Z.Y., Zeng, Y., Zheng, N.J., Luo, L., Xiao, H.W., Xiao, H., 2020b. Fossil fuel-related emissions were the major source of NH_3 pollution in urban cities of northern China in the autumn of 2017. Environ. Pollut., 113428

Zhou, Y.H., Xiao, H.Y., Guan, H., Zheng, N.J., Zhang, Z.Y., Tian, J., et al., 2020. Chemical composition and seasonal variations of PM2.5 in an urban environment in Kunming, SW China: importance of prevailing westerlies in cold season. Atmos. Environ. 237, 117704.